

Field-Cycling NMR Relaxometry with Spatial Selection

Kerrin J. Pine, Gareth R. Davies and David J. Lurie

Aberdeen Biomedical Imaging Centre, University of Aberdeen, Aberdeen, Scotland, United Kingdom

E-mail: k.pine@abdn.ac.uk

Phone: +44 1224 553199

Fax: +44 1224 552514

Abstract

Fast field-cycling (FFC) MRI offers access to sources of endogenous information not available from conventional fixed-field imagers. One example is the T_1 dispersion curve: a plot of T_1 versus field strength. We present a pulse sequence that combines saturation-recovery/inversion-recovery T_1 determination with field-cycling and point-resolved spectroscopy (PRESS) localization, enabling the measurement of dispersion curves from volumes selected from a pilot image. Compared with a non-selective sequence, our method of volume selection does not influence measurement accuracy, even for relatively long echo times and in the presence of B_1 non-uniformity. The measured voxel profile, while not ideal, corresponds with that expected from the image slice profile. On a whole-body FFC scanner with 59 mT detection, the sensitivity of the experiment is sufficient to reveal distinctive “quadrupole dips” in dispersion curves of protein-rich human tissue *in vivo*.

Keywords: field-cycling; T1 relaxometry; nuclear magnetic resonance

Introduction

Conventional MRI requires a stable magnetic field held constant throughout the imaging process. In fast field-cycling MRI (FFC MRI) the field is switched between two or more values in a time of the same order as T_1 , usually by varying the current flowing through a resistive magnet or resistive-permanent magnet hybrid. In this way, the spin ensemble can be allowed to evolve at a range of fields, before returning to the scanner's native field strength for detection. Through study of the strong dependence of tissue T_1 on field strength, field-cycling investigations can reveal information not accessible to conventional fixed-field imagers. In this way, FFC MRI has the potential to increase the diagnostic information available from MRI.

One such use is the characterization of proteins and other biopolymers, which exhibit pronounced reductions in T_1 at certain well-known NMR frequencies, due to interactions with the quadrupolar nucleus ^{14}N (1). On a T_1 dispersion curve (plotting T_1 versus evolution field B_{0E}), these so-called "quadrupole dips" have previously been observed in leeches (2), collagen fibres (3), multiple sclerosis plaques (4) and human tissues *in vivo* (5, 6), among others. The dips provide information about the sample's protein concentration (7). *In vivo* field-cycling relaxometry studies have been limited to determining the T_1 of entire samples without spatial localization as well as image-based methods, which require the collection of a T_1 weighted image at each field-cycling step.

In the work of Carlson et al. (5), an electromagnet was switched on for a short time and then switched off during conventional MR imaging. Signal intensity within a region of interest was averaged and a global fit of the data was used to estimate T_1 as a function of field strength. Because of the need to acquire data in phase encoded steps at each field point, total imaging time was lengthy.

In this work, we have explored the use of image-selected volume-localized FFC relaxometry, which offers the advantages of less partial-voluming than whole-sample relaxometry, as well as better SNR and faster acquisition times than image based techniques. Signal localization is achieved by the well-known point resolved spectroscopy (PRESS) method (8), in which three

selective RF pulses are used in sequence in the presence of three orthogonal magnetic field gradients.

Theory

A field-cycling, interleaved inversion-recovery / saturation-recovery pulse sequence was used to measure T_1 values by a two-point method, with PRESS selecting the targeted volume. The sequence is shown in Fig. 1. A 10 ms adiabatic fast passage inversion is applied on alternate executions to allow T_1 measurement by inversion-recovery. This is followed by an evolution period at the field strength of interest B_{0E} with duration T_{evol} of the order of the sample's T_1 . After a field settling delay T_d , a soft 90° RF pulse is applied in the presence of a field gradient, followed by two 180° RF pulses applied with orthogonal gradients. The gradients extend briefly before and after each 180° pulse in order to spoil any unwanted transverse magnetization. The resulting spin echo from a selected volume is acquired. After a delay to allow complete longitudinal recovery, the sequence is repeated without AFP inversion. In order to collect data for a T_1 dispersion curve, the sequence is repeated at a range of B_{0E} values.

For simplicity in our analysis, we assume monoexponential decay and that inhomogeneity in B_0 and RF is negligible. As the field switching times are short in relation to T_1 , we do not account for the variation in relaxation rate during field ramps, and the ramps are approximated by a step function.

Let M_0 and M_{0E} be the thermal equilibrium magnetization at observation and evolution fields B_0 and B_{0E} , respectively. T_1 is the spin-lattice relaxation time in the evolution field and T_{1obs} is the value of T_1 at the observation field. Let M_z and M_{xy} be the respective instantaneous longitudinal and transverse components of the magnetization in the rotating frame. For the non-inversion case after evolution time T_{evol} and field settling delay T_d ,

$$M_z^{NI} = M_0 + (M_{0E} - M_0) \exp\left(\frac{-T_d}{T_{1obs}}\right) - (M_{0E} - M_0) \exp\left(\frac{-T_d}{T_{1obs}} - \frac{T_{evol}}{T_1}\right) \quad [1]$$

For the inversion-recovery case, the initial magnetization is identical in magnitude but oppositely signed. If T_a is the delay between inversion and field switching,

$$M_z^I = M_0 + (M_{0E} - M_0) \exp\left(\frac{-T_d}{T_{1obs}}\right) - \left\{ M_{0E} \left[1 - 2 \exp\left(\frac{-T_a}{T_{1obs}}\right) \right] - M_0 \right\} \exp\left(\frac{-T_d}{T_{1obs}} - \frac{T_{evol}}{T_1}\right) [2]$$

Solving for T_1 , the final result is:

$$T_1 = T_{evol} / \ln(b) \text{ where}$$

$$b = \left\{ \frac{M_z^{NI} + M_z^I}{M_z^{NI} - M_z^I} + 1 + \left(\frac{B_{0E}}{B_0} - 1 \right) \exp\left(\frac{-T_a}{T_{1obs}}\right) \right\} / \left\{ \left[\frac{B_{0E}}{B_0} - 1 + \exp\left(\frac{-T_d}{T_{1obs}}\right) \right] \exp\left(\frac{-T_a}{T_{1obs}}\right) \right\} [3]$$

Volume localization begins with the selective 90° pulse, which transfers longitudinal magnetization into the transverse plane. Therefore, the measured T_1 is independent of spin-lattice relaxation during the PRESS part of the pulse sequence. The requirement for knowledge of T_1 at the observation field presents no difficulty as it is straightforward to first conduct the experiment with equal observation and evolution field strengths.

Methods

The imager used for these experiments was a home-built, whole-body, field-cycling MRI system (9). The detection field is provided by a whole-body permanent magnet with a 59 mT vertical field and clear bore of 65 cm (Field Effects Inc., MA, USA). A co-axial resistive saddle-shaped magnet (Magnex Scientific Ltd., UK) allows field-cycling through field compensation.

All functions of the system are controlled by a commercial MRI console (SMIS Ltd., UK). Magnetic field gradient magnitudes and RF frequency offsets are calculated automatically by the system software after marking the volume of interest on one or more pilot images.

RF pulses for volume selection were of 5-lobe sinc in shape and of 4.5 kHz bandwidth. The transmit/receive coil used was a split-solenoid RF coil assembly made from 6 mm diameter copper pipe with length 12 cm and diameter 32 cm, tuned to 2.5 MHz. The coil is equipped with

trimmer capacitors allowing fine tuning and matching to be carried out with the sample in place. The assembly is housed in a cylindrical copper foil RF shield.

During the acquisition period, the echo signal is sampled at twenty points. After averaging of a configurable number of excitations, the average magnitude of the twenty points is retained and used for calculation of T_1 . The repetition time TR is chosen in an iterative manner to exceed five times the expected T_1 of the sample.

For the purpose of comparison, relaxometry was also performed using a commercial fast field-cycling relaxometer (SMARtracer, Stelar s.r.l., Italy).

Results

A variety of experiments was carried out to confirm that the measured T_1 is accurate and to investigate the effects of positioning and longer echo times. A robust sequence for volume-localized field-cycling relaxometry will produce T_1 measurements consistent with non-localized techniques. At the imager's observation field of 59 mT and at 21°C, the T_1 of a sample containing approximately 125 ml of 0.20 mM manganese chloride solution was measured by AFP- τ -90° inversion-recovery (τ 250 ms). By the 2-point method, the measured T_1 was determined to be 222.3 ± 0.2 ms (mean \pm SD, $n = 8$). After gradient echo imaging, a pilot image was used to place a 40 x 40 x 40 mm voxel centrally enclosing the sample bottle. Our sequence was then used at fixed-field to determine a volume-localized T_1 of 222.5 ± 3 ms, which corresponds closely with the non-selective result.

To evaluate robustness, volume-localized dispersion curves were compared with a non-localized version of the same sequence, where the PRESS section was replaced by a hard 90° acquisition. Nine bottles of varying concentrations of manganese chloride and copper sulphate in water were inserted into a volume-selection phantom such that they formed a 3 x 3 grid and they were imaged by a gradient echo pulse sequence (Fig. 2). Dispersion curves were collected with 40 x 40 x 40 mm voxels placed within each bottle volume using the volume-localized sequence, and

separately with the non-localized version of the pulse sequence on one bottle at a time in the imager. No significant variations in the dispersion curves were noted.

For the solution of 0.2 mM manganese chloride, three dispersion curves were compared: from the bottle selected from the multi-compartmental phantom using localized relaxometry; from the sole bottle using conventional whole-sample inversion-recovery and from a commercial small-sample relaxometer. Relaxation time T_1 and its dispersion are comparable between the three methods.

Aside from robustness, an important consideration in any localization application is quantifying the accuracy with which the volume is selected. One useful measure is the voxel profile, in which the voxel selection is moved across the boundaries of a homogenous test object of known dimensions, akin to the image slice profile experiment in MRI. The sample was a Perspex tank (dimensions 189 x 76 x 72 mm) partially filled with deionised water and sufficient copper sulphate to reduce T_1 to approximately 120 ms. To examine the voxel profile in the z -direction (along the bore of the imager), the tank was moved through z in fixed steps with a static 30 x 30 x 30 mm voxel selected to remain well within the object in the x - y plane. At each step, the saturation-recovery signal was acquired five times and averaged. This was then compared to the convolution of the tank length and the measured image slice profile in the same dimension. Due to truncation of the sinc pulses to five lobes, the voxel profile (Fig. 3a) is not rectangular yet it closely matches that predicted by the image slice profile.

The voxel profile cannot simply be measured by keeping the tank static and moving the voxel, because of the confounding factors of B_1 inhomogeneity and coil efficiency as the offset frequency is swept. The same tank was held stationary in the imager while a voxel was swept along the direction of the imager's bore. The measured T_1 remained relatively unaffected, staying within 3% while the voxel was contained entirely within the tank volume (data not shown).

In order to confirm our expectation that measured T_1 is insensitive to choice of echo time TE, the sequence was executed repeatedly at fixed field (59 mT) with the tank in the imager and echo times ranging from 34 ms to 200 ms. The results (Fig. 3b) show no significant variation in T_1 ,

even when the value of TE approaches and exceeds that of T_2 (which is equal to T_1). This is encouraging, as PRESS typically necessitates the use of longer echo times compared to other localization techniques. Accuracy and precision decline at longer TE values due to the decay of signal from spin-spin relaxation.

Biological samples were investigated as follows. In a first experiment, four hen eggs were placed into the imager, two of which had been cooked by immersion in boiling water for ten minutes. After pilot imaging, 40 x 40 x 40 mm voxels were located over raw and cooked eggs. The dispersion curves clearly showed quadrupole dips for the cooked eggs but not for the raw eggs (data not shown). This is expected due to protein immobilization and cross-linking in the albumin protein.

A single cooked hen egg was placed into a smaller RF coil (length 10 cm and diameter 7 cm) in order to achieve an optimum filling factor. With the improved SNR, it was possible to collect dispersion curves for yolk and albumen separately (Fig. 4). Significant quadrupole dips centered on 49 mT and 65 mT can be seen on the dispersion curve obtained from albumen.

In a second proof-of-principle experiment, measurements were made of the thighs of a human volunteer. A gradient-echo pilot image was obtained and regions-of-interest for localized relaxometry were placed inside and outside regions of muscle. The image and the resulting dispersion curves are shown in Fig. 5. As expected due to the higher protein concentration, quadrupole dips were more evident for the muscle-containing voxel.

Discussion

We have presented a successful implementation of volume-localized field-cycling relaxometry with sufficient sensitivity to demonstrate quadrupole dips in hen eggs and *in vivo* in human thigh muscle. The relatively long time between excitation and acquisition in PRESS localization (32 ms in our sequence) did not impede the measurement of T_1 , even for echo times of the order of the sample's T_2 . Quality control measurements provide assurance that the volume selection does

not adversely affect T_1 measurement, that the voxel profile is measurable, and that T_1 measurement is robust in the presence of B_0 and B_1 field inhomogeneity.

Field-cycling imaging and relaxometry may provide information about biological processes not available from conventional scanners. Image-based relaxometry methods require the collection of a sequence of images at each field step. By contrast, localized field-cycling with two-point inversion-recovery involves just two sequence repetitions and significantly faster acquisition times. Our approach allows the collection of data for only the volume of interest and therefore avoids a compromise between SNR and partial-voluming.

T_1 dispersion curves of biological samples reveal distinctive dips due to strong coupling between backbone protons and the quadrupolar nucleus ^{14}N in immobilised proteins. The location of these dips is in agreement with previous work. As the depth of the dips provides information about protein concentration (7), localized field-cycling relaxometry could find applications in protein measurement or form the basis of new types of contrast in clinical MRI.

Acknowledgements

The authors acknowledge financial support for the FFC MRI project from Research Councils UK and the Engineering and Physical Sciences Research Council, under the Basic Technology scheme (grant number EP/E036775/1).

References

1. Winter F, Kimmich R. Spin lattice relaxation of dipole nuclei ($I=1/2$) coupled to quadrupole nuclei ($S=1$). *Mol Phys* 1982; **45**: 33-49.
2. Kimmich R, Nusser W, Winter F. In vivo NMR field-cycling relaxation spectroscopy reveals $^{14}\text{N}^1\text{H}$ relaxation sinks in the backbones of proteins. *Phys Med Biol* 1984; **29**: 593-596.
3. Peto S, Gillis P, Henri VP. Structure and dynamics of water in tendon from NMR relaxation measurements. *Biophys J* 1990; **57**: 71-84.

4. Rinck PA, Fischer HW, Elst LV, Haverbeke YV, Muller RN. Field-cycling relaxometry: medical applications. *Radiology* 1988; **168**: 843-849.
5. Carlson JW, Goldhaber DM, Brito A, Kaufman L. MR relaxometry imaging. Work in progress. *Radiology* 1992; **184**: 635-639.
6. Lurie DJ. Quadrupole Dips Measured by Whole-Body Field-Cycling Relaxometry and Imaging. In: Proceedings of the 7th Annual Meeting of ISMRM, Philadelphia, USA, 1999. p. 653.
7. Jiao X, Bryant RG. Noninvasive measurement of protein concentration. *Magn Reson Med* 1996; **35**: 159-161.
8. Bottomley PA. Spatial localization in NMR spectroscopy in vivo. *Ann N Y Acad Sci* 1987; **508**: 333-348.
9. Lurie DJ, Foster MA, Yeung D, Hutchison JM. Design, construction and use of a large-sample field-cycled PEDRI imager. *Phys Med Biol* 1998; **43**: 1877-1886.

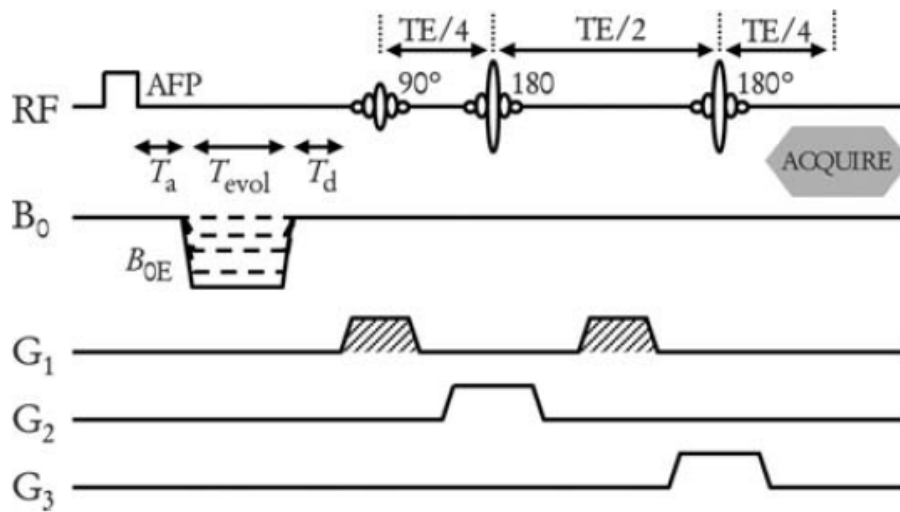


Figure 1: Pulse sequence diagram. AFP inversion occurs on every second execution. Gradients can be applied in any three orthogonal directions. The signal acquired is an echo with centre located TE after the 90° excitation.

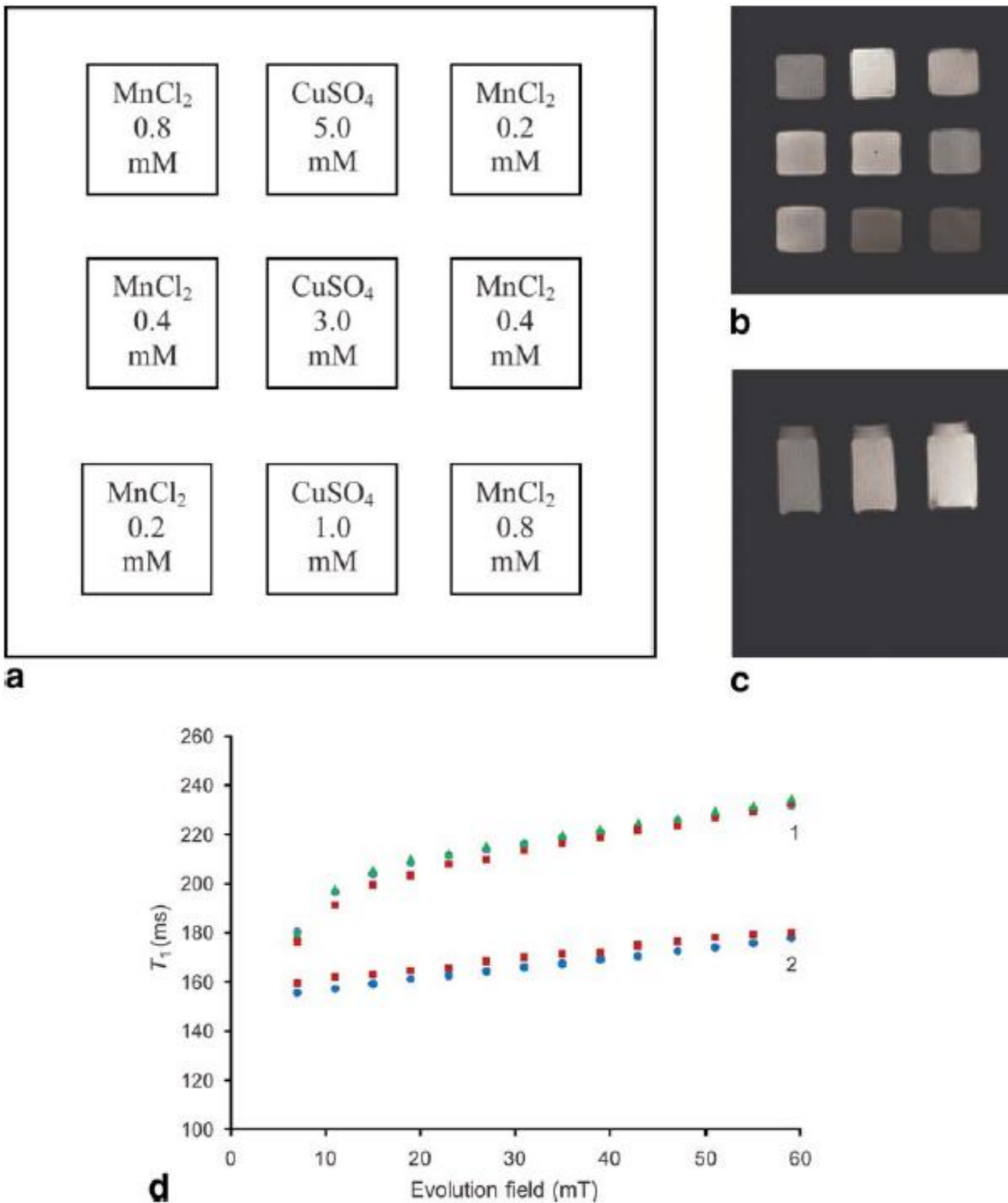


Figure 2

Schematic of multi-sample phantom (a) and gradient echo images, transaxial (b) and coronal (c). TR 300 ms, TE 32 ms, field of view 250 mm, slice thickness 40 mm, 4 averages. (d) Curves show comparable relaxation times and dispersion for [1] 0.2 mM MnCl₂ and [2] 3 mM CuSO₄ solutions. Relaxometry data was collected with conventional whole-sample IR (circles), volume-localized IR (squares), and by a commercial relaxometer for the solution of 0.2 mM MnCl₂ only (triangles).

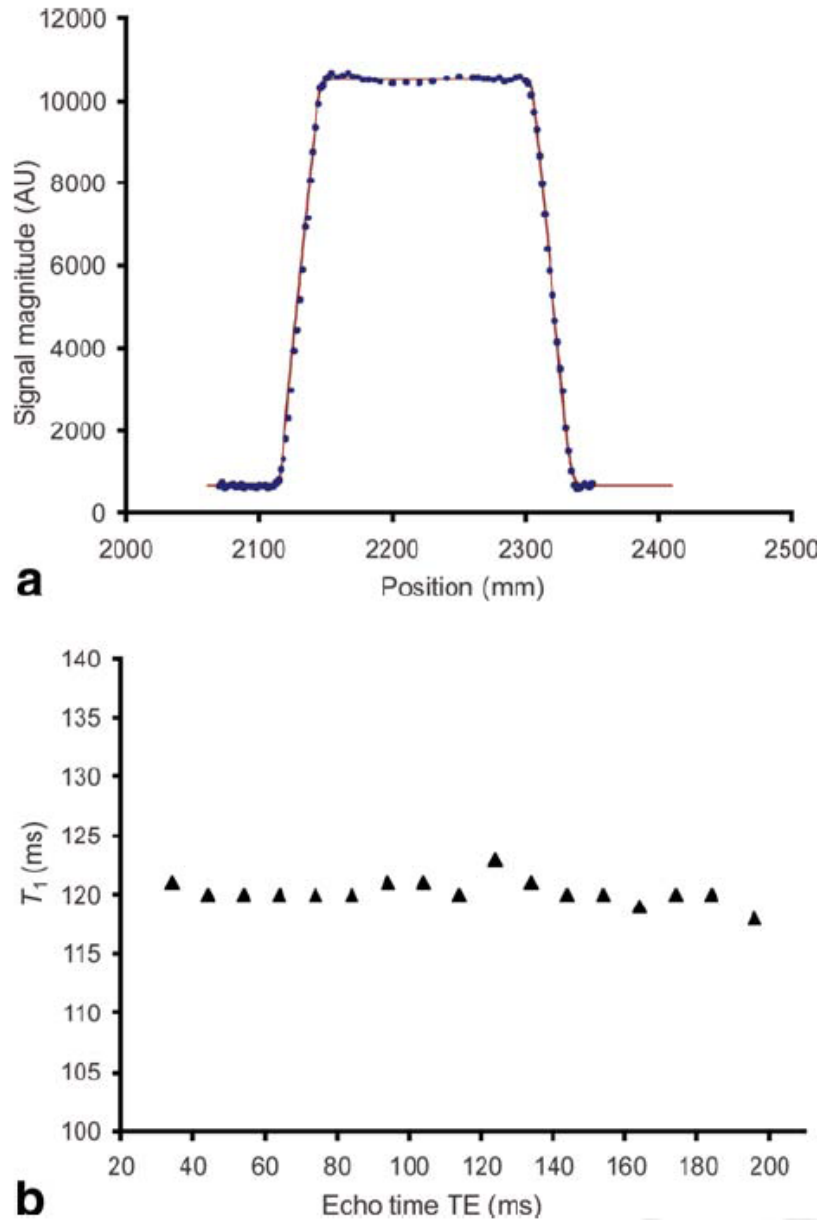


Figure 3

(a): A tank containing copper sulphate solution (dimensions 189 x 76 x 80 mm) was moved through the imager along the bore, while acquiring the average magnitude of the sampled echo from a fixed 30 x 30 x 30 mm voxel (circles). The convolution of the image slice profile (measured with 30 mm slice width along the bore by the well-known opposing wedge method) and tank length is also shown (solid line).

(b): Measured T_1 with localized relaxometry of same tank as a function of echo time. Voxel size 40x40x40mm, TR 920 ms, T_{evol} 100 ms.

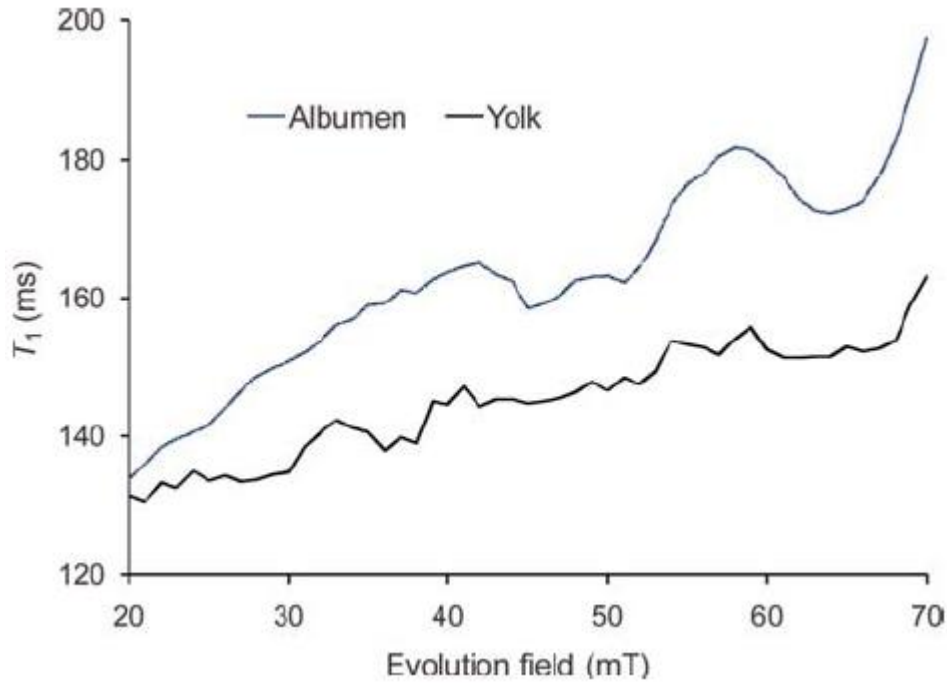


Figure 4: Dispersion curves for a boiled hen egg with voxels located in regions of egg albumen and egg yolk. Voxel size 20 x 20 x 20 mm, TR 1100 ms, evolution time 200 ms (albumen) and 120 ms (yolk), 3 point moving average.

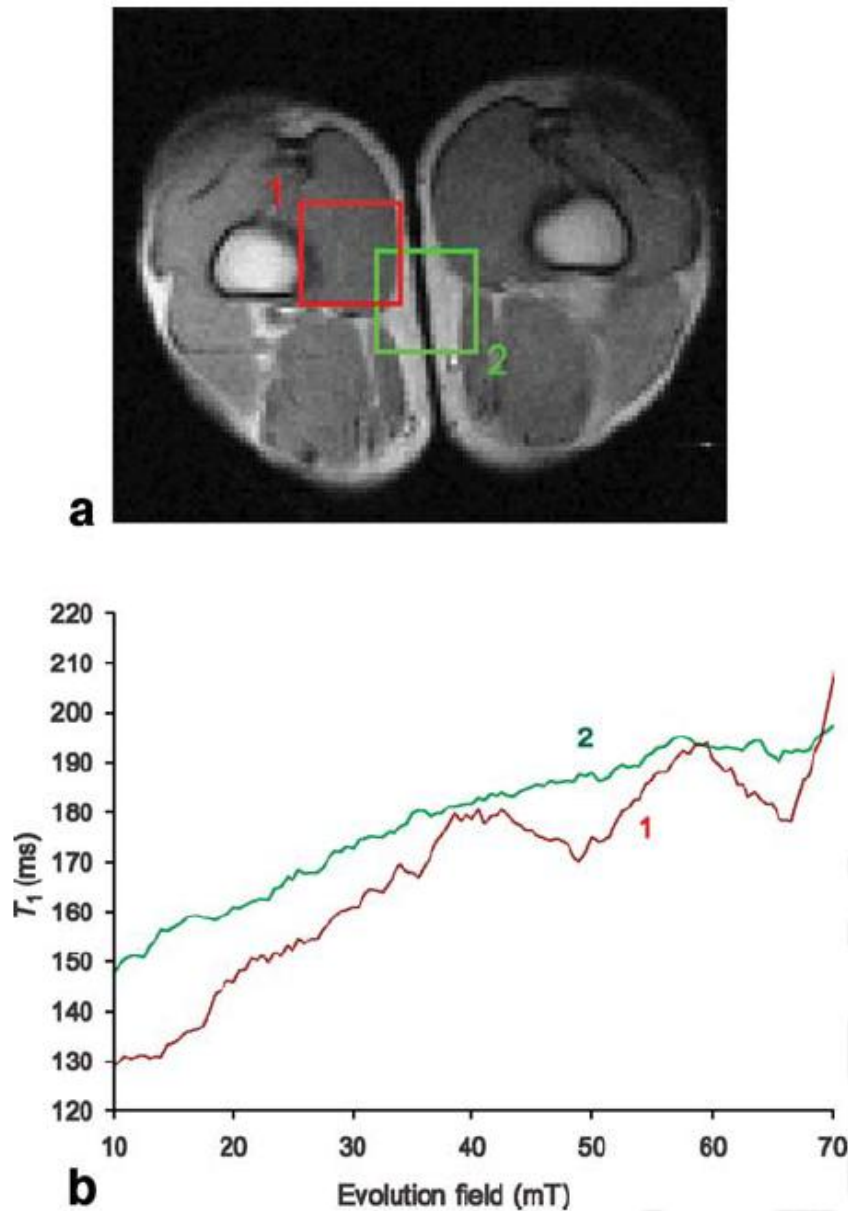


Figure 5

(a): Gradient echo images showing the selection of regions inside [1] and outside [2] of human thigh muscle. TR 300 ms, TE 32 ms, field of view 250 mm, slice thickness 40 mm, 4 averages.

(b): Dispersion curves for the selected regions. Quadrupole dips are more evident for the muscle-containing region [1], due to the high concentration of protein. Voxel size 40 x 40 x 40 mm, TR 2 s, evolution time 250 ms. 3 point moving average.